

Squall Lines Organisation in Tropics

Sophie Abramian, Caroline Muller, Camille Risi

¹Laboratoire de Météorologie Dynamique de l'ENS Paris

Key Points:

- enter point 1 here
- enter point 2 here
- enter point 3 here

8 **Abstract**

9 Using a cloud resolving model, we attempt to clarify the physical processes responsible
 10 for the organization of deep clouds into squall lines in the tropics. To do so, we impose
 11 a vertical wind shear, and investigate the response of deep convection to different shear
 12 strengths in radiative convective equilibrium. As the magnitude of the shear increases,
 13 the convection becomes more and more organized into a line, perpendicular to the shear.
 14 It is due to the interaction of the low-level shear with the cold pools associated with con-
 15 vective downdrafts. Beyond a certain shear, called optimal shear, the line tends to ori-
 16 ent at an angle to the shear. The existing literature suggests that this angle conserves
 17 the projection of the shear on the direction perpendicular to the squall line near the op-
 18 timal value, a hypothesis that we further investigate here. In this work, we propose a
 19 systematic method, based on image auto-correlation, to determine the angle of the squall
 20 line with respect to the shear. We highlight the existence of the sub-critical and super-
 21 critical regime, as predicted by earlier studies. In the sub-critical regime, squall lines are
 22 indeed perpendicular to the shear. Yet, angles of squall lines in the super-critical regime
 23 do not clearly correspond to the conservation of the projected component of the shear
 24 near the optimal value. In particular, squall lines often remain more perpendicular to
 25 the shear than expected. We thus investigate the balance between shear and cold pool
 26 winds to explain this difference. Using statistical methods on extreme events, we find
 27 that this difference is due to an intensification of cold pool potential energy with shear.
 28 Cold pool intensification allows the squall line to better resist to the shear, and thus re-
 29 duces its angle of orientation. This new feature leads us to conclude that two mechanisms
 30 maintain a squall line in wind shear : the orientation of clouds and the intensification
 31 of cold pools.

32 **Plain Language Summary**

33 [enter your Plain Language Summary here or delete this section]

34 **1 Introduction**

35 **1.1 Squall line organisation in tropics**

36 Squall lines are a particular form of spatial organisation of clouds, where they ag-
 37 gregate into a band of thunderstorms several hundred kilometres long. This organisa-
 38 tion is associated with extreme meteorological events, including very heavy precipita-
 39 tion, and many studies question the consequences of global warming on the intensifica-
 40 tion of these phenomena. In particular, O'Gorman and Schneider find that the rate of
 41 increase of tropical precipitation extremes in the third Coupled Model Intercomparison
 42 Project (CMIP3) climate model simulations ranged from 1.3% to 30% depending on the
 43 climate model. A recent study (Muller 2013) showed that rainfall associated with squall
 44 lines would increase with increasing mean surface temperature by 15%.

45 Yet, if global warming leads to more intense thunderstorms, these same convective
 46 systems also participate in the warming. This is known as cloud feedback, the impact
 47 of increased cloud cover on surface temperatures. The tropics, equatorward of 30°, ab-
 48 sorb, on average, about 400 W m-2 of solar radiation, of which less than 20 is exported
 49 to the extratropics (Popke et al. 2013) and therefore play a crucial role in climate sen-
 50 sitivity. However, the modelling of convective organisation in the tropics remains the source
 51 of much of the uncertainty surrounding predictions of climate variability (Bony et. al
 52 2015).

53 Indeed, mesoscale systems are not taken into account in most global climate pre-
 54 diction models, since their size generally corresponds to the size of the global grid. MCS
 55 should be parameterised by sub-grid terms in the model equations, a challenge that is

56 still ongoing, often referred to as breaking the cloud parametrization deadlock (Randall
57 et al. 2003).

58 Our study aims at clarifying the physical processes related to the organization of
59 clouds into squall lines in order to contribute to the resolution of the above-mentioned
60 problems. The squall line organisation is known to be a response to vertical wind shear
61 forcing and a large literature has already been written on this subject, starting with sev-
62 eral squall line observation campaigns. The first major campaign was the GATE cam-
63 paign, Bluestein et al. 84 conducted one of the first squall line measurements in Okla-
64 homa and were able to draw four main classes of analysis of this system according to their
65 development. For severe lines, the most frequent development observed was that of back-
66 builind, i.e. a periodic appearance of a new cell upstream, relative to cell motion, from
67 an old cell and the resulting merger of the new cell with the old cell as the former ex-
68 pands in area. The formation of squall lines, in this case, turns out to be the constant
69 triggering of convective cells.

70 Based on these observations, a theory of tropical squall lines was constructed by
RKW, which is still the standard for their development today. RKW starts from the fact
71 that in the presence of wind shear, deep convection cannot develop because the updraft
72 is tilted. To allow clouds to break through, the wind shear must be counterbalanced. Cold
73 pools play this crucial role. Convective cells therefore develop at the edges of the pools,
74 and thus draw arcs and lines. The periodic appearance of a new cell observed by Bluestein
75 is therefore the manifestation of a permanent appearance of a cold pool.

76 This paper highlights three regimes, the sub-critical regime, where density currents
77 dominate, the optimal regime where the cold pool shear equilibrium is reached, and fi-
78 nally the super-critical regime where shear dominates. In the latter case, the squall lines
79 tend to orient themselves as the shear increases. The literature suggests that the orien-
80 tation of the line keeps the projected component of the shear close to the optimal value.

82 The RKW theory still raises some questions, and its highly idealised aspect is some-
times questioned. Robe and Emmanuel 2010 investigated the evolution of the squall line
83 organisation for a range of shear. The rotunno theory is qualitatively verified but it is
84 still difficult to assess quantitatively the organisation of the lines. Since they often form
85 cloudy arcs, defining an orientation remains an obstacle. Another aspect that challenges
86 the theory of rkw, suggested this time by Alfaro 2016, is that the strongest squall lines
87 may produce the most intense cold pools and can then shift the optimality regime and
88 also modify the orientation of the lines.

89 The recent development of numerical tools for convection modelling allows us to
go one step further in the investigation of squall lines. The objective of our study is to
90 quantify the approaches of RKW, Robe et al and Alfaro, in order to determine whether
91 the cold pool and shear balance is sufficient to describe squall lines. More precisely, we
92 asked ourselves two main questions

93 to determine squall line orientation ? does this angle evolve with shear ? do cold
94 pool characteristics change with shear?

97 1.2 State of the art

98 1.3 Problematic questions

99 2 Methodology

100 2.1 Cloud Resolving Model SAM

101 We have simulated several cases of squall lines using the CRM SAM. This model
102 is based on a non-hydrostatic and anelastic formulation of atmospheric flows. It has the
103 particularity to cover a large range of scale, and is easily adapted to the study of mesoscale

systems such as squall lines. The prognostic thermodynamic variables of the model include total nonprecipitating water (vapor 1 cloud water 1 cloud ice) and total precipitating water (rain 1 snow 1 graupel). The mixing ratio of cloud water, cloud ice, rain, graupel, and snow is diagnosed from the prognostic variables using a temperature-dependent partition between liquid and ice phases. The frozen moist static energy, which is the sum of the liquid/ice water static energy and the total condensate amount times the latent heat of vaporization, is conserved during moist adiabatic processes in the model, including the freezing and melting of precipitation. The model is run to radiative convective equilibrium, and once equilibrium is reached the organisation of squall line is analyzed.

All simulations are three-dimensional on a square, doubly periodic horizontal domain. The vertical grid has 53 levels (capped at 17 km with a rigid lid), with the first level at 37.5 m and grid spacing gradually increasing from 80 m near the surface to 400 m above 6 km, and a variable time step (10 s or less to satisfy the Courant–Friedrichs–Lowy condition). The surface fluxes are computed using Monin–Obukhov similarity. To reduce gravity wave reflection and buildup, Newtonian damping is applied to all prognostic variables in the upper third of the model domain.

2.2 Simulation set-up

Vertical shear is imposed to organize the convection into squall lines. When no shear is imposed, convection develops randomly over the domain, similar to popcorn formation. The shear will cause a symmetry break in the domain, and prevent deep convection. For convection to develop, this shear must be counterbalanced. Density currents are therefore the key element in the development of deep convection in the presence of a shear, since by spreading radially, the cold pool will counterbalance the shear vorticity and restore local symmetry; we speak of a vorticity dipole. Thus, when a cold pool is formed, we observe the triggering of vertical convective cells, which form the clouds. These will then precipitate, and form in turn cold pools. The clouds are formed from one to another, at the edge of the cold pool and draw a succession of clouds arc. Moreover, the arcs are all oriented in the same way. Robe and Emmanuel 2001 hypothesized that the cold pool shear equilibrium selected an orientation of the arcs.

In our study, we looked for shear profiles to observe grain lines in the subcritical, optimal and supercritical regimes. Robe Emmanuel 2001 suggests that the shear depth should be of the order of magnitude of the cold pool height. RKW estimates the optimal shear at ... or 10m/s in our case. A linear shear profile was chosen for a shear depth of 1000m/s. We then varied the basal velocity from one case to another, which makes 9 different cases, from $U=0\text{m/s}$ to $U=20\text{m/s}$ with steps of $\Delta u = 2.5\text{m/s}$.

2.3 Overview of squall lines

3 Validation of the theoretical orientation of squall lines

3.1 Squall lines orientation theory

Vertical shear is imposed to organize the convection into squall lines. When no shear is imposed, convection develops randomly over the domain, similar to popcorn formation. The shear will cause a symmetry break in the domain, and prevent deep convection. For convection to develop, shear must be counterbalanced. Density currents are therefore the key element in the development of deep convection in the presence of a shear, since by spreading radially, the cold pool will counterbalance the shear and restore local symmetry; we speak of a vorticity dipole. Thus, when a cold pool is formed, we observe the triggering of vertical convective cells, which form the clouds. These will then precipitate, and form in turn cold pool. The clouds are formed from one to another, at the edge of the cold pockets and draw a succession of clouds arc. Moreover, the arcs are

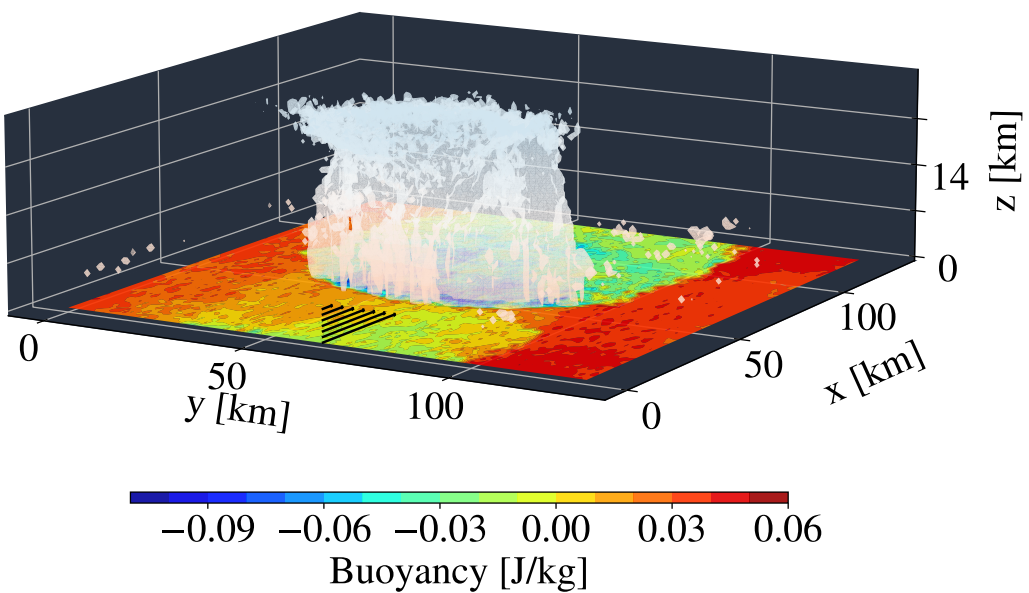
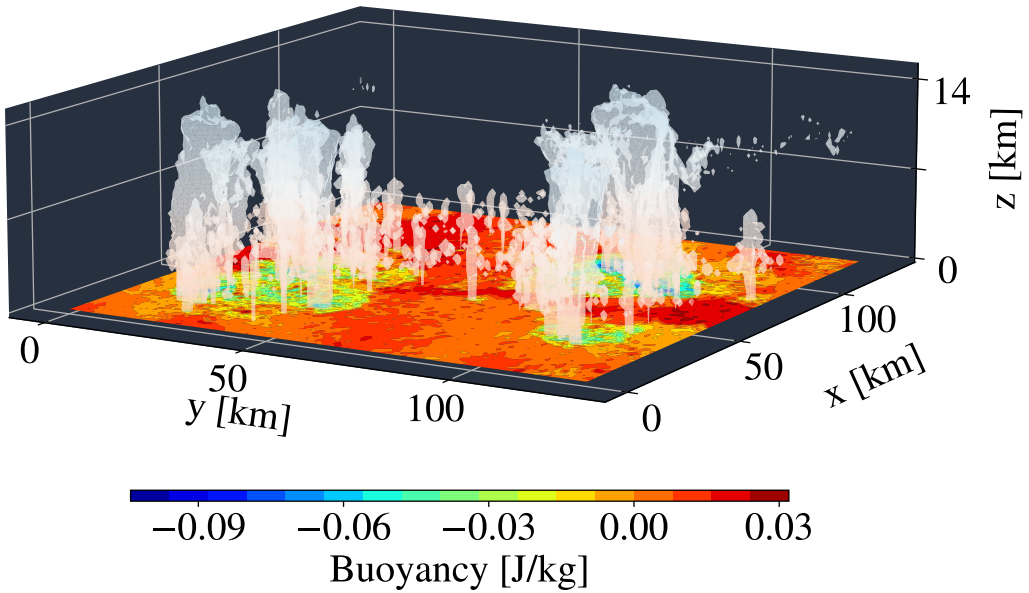
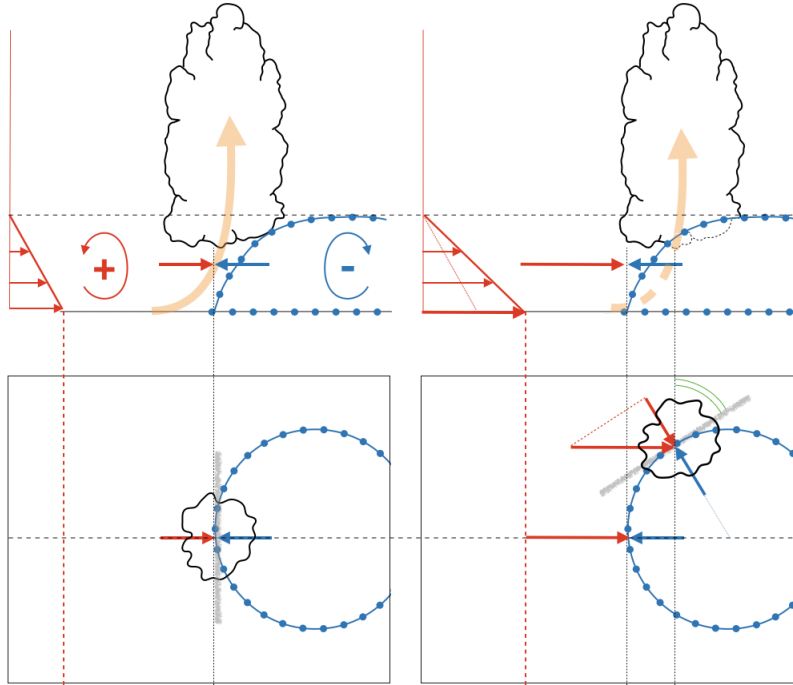


Figure 1. Top. In the absence of shear, we observe, in yellow, a random convection called 'popcorn'. This is an isosurface $QN+QP=0.1\text{g}/\text{kg}$. The orange shading allows to place it in altitude. On the ground, the buoyancy at the lowest atmospheric level is shown. On top, the precipi-

**Figure 2.** caption

all oriented in the same way. Robe and Emmanuel 2001 hypothesized that the cold pocket shear equilibrium selected an orientation of the arcs.

Up to now, we will speak of a velocity balance rather than a vorticity balance. This is possible in our case because we impose a linear shear profile, and thus the vorticity is proportional to the velocity; moreover, the velocity profile of the pockets can be modeled to the first order as linear to the also.

Let us imagine a shear wind going from west to east, which encounters a cold pool. This pocket is assumed to be circular, and its spreading speed radial. On its western front, the pocket opposes the shear, and the strength of the wind felt by the pool is all the greater on the western extreme of the pool.

This is because the velocity balance between the shear and the cold pool is always radially projected. Thus, the projected wind shear is maximum in the west-east direction, and decreases at the edges of the pool, while the pool propagation speed is radially uniform. When the wind speed is equal to the propagation speed of the pools, we are in the optimal regime, and the equilibrium, i.e. the location of the convective cell triggering, is on the extreme west front of the pool. When the wind speed is lower than the propagation speed of the pool, then the equilibrium place is also on the extreme western front of the pool to maximize the wind strength. This is referred to as a subcritical velocity regime. On the contrary, when the wind becomes stronger than the pool, the equilibrium moves along the edge of the pool, either north or south; this is the supercritical regime. There is thus an always selected position, which depends only on the cold pool propagation speed and the basal shear velocity.

The literature suggest that cold pool velocity is constant, regardless of the imposed velocity profile. Thus, for a simulation set where only the shear profile changes, the pool properties do not vary. In this case, the nature of the regime depends only on the basal

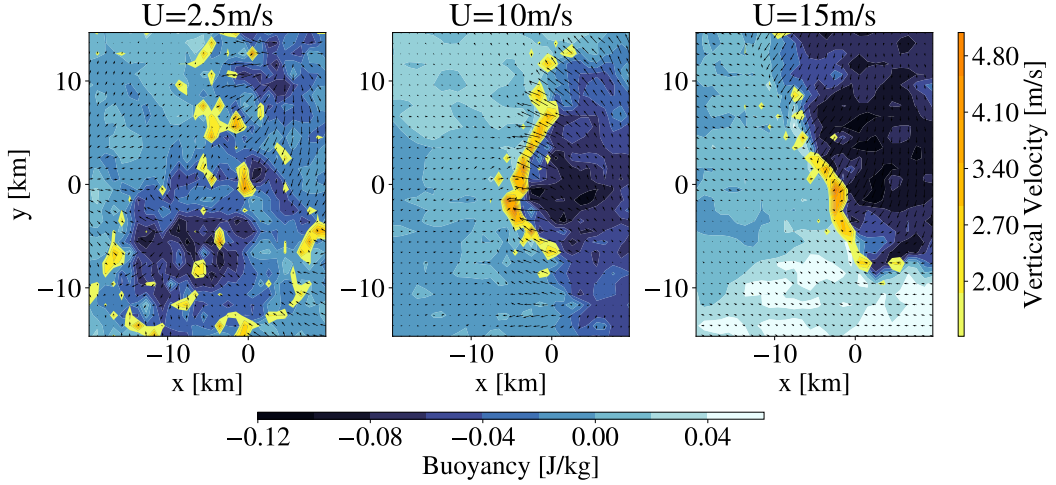


Figure 3. Buoyancy at the lowest atmospheric level (blue), vertical velocity field W at 250m (orange) and surface velocity field (black vectors), for the three cases: control, optimal and super-critical. We can see that convection is triggered at the edge of the pool, when a shear is applied. Moreover, the radial spreading of the cold pools is confirmed.

shear velocity. The position of the convective cell initiation is parameterized by the arc along the pool. The squall line is thus formed on the tangent of the pocket at this position.

In short, the triggering position of the cells is always at the edge of the cold pocket, and as the shear rate increases, so does the angle to the horizontal, in order to keep the projection along this direction close to the propagation speed of the cold pocket. A cloud mass develops on the tangent to the pocket in this position. These clouds will precipitate, form a new cold pocket and repeat the process. The direction of the tangent is maintained throughout the phenomenon, and on a large scale forms a squall line of several tens of kilometers.

In the following, we propose a new method to measure automatically squall line orientation, based on image auto-correlation.

3.2 Automatic measurement of squall lines orientation

Squall lines orientation refers to their position in relation to its surroundings. Several angle definitions are possible for describing this particular direction, so we chose to define the angle with respect to the latitudinal direction, which allows to have a reference angle at 0 when the line is perpendicular to the wind flow.

Our aim is to determine this angle by an automatic and objective method. To do so, we asked ourselves what was the fundamental property of a geometrical line. A naive way of considering a line is its invariant by translation along its direction. A useful mean to detect invariant and regularity of image is to use an auto-correlation filter. The auto-correlation image of a 2d variable is defined by :

$$\mathcal{A}_F(u, v) = \mathbb{E}(F(x, y)F(x + u, y + v)) \quad (1)$$

In the case of a line, or more realistic here a 2d-band, the auto-correlation is characterized by the product of two quadratic forms. In fact, if the band has for main axis

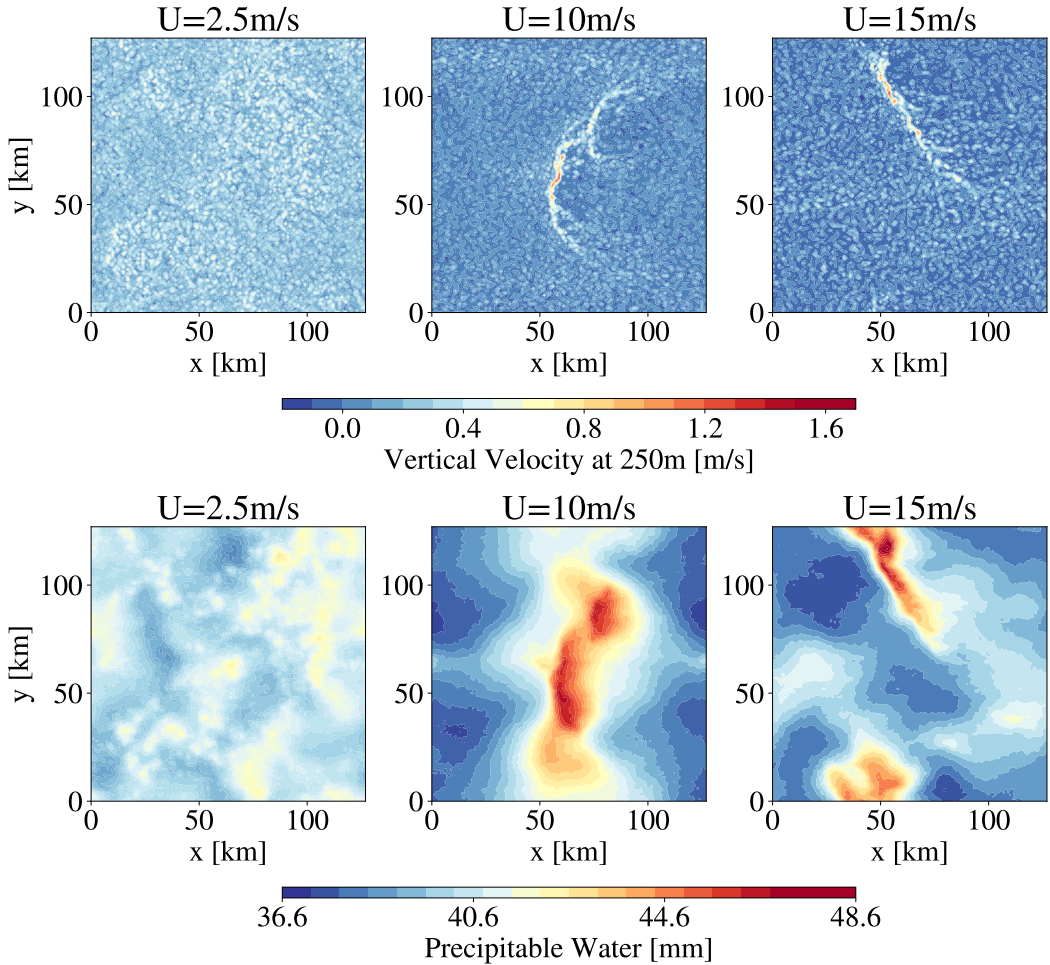


Figure 4. Evolution of the vertical velocity field W at 250m, and the PW field for different shear values. In the absence of shear, no squall lines are observed. For $U=10\text{ m/s}$, arcs perpendicular to the wind are formed. For $U=15\text{ m/s}$, the line is oriented with respect to the vertical. The evolution of W and PW accounts for the same phenomenon, the line organization. However, PW images provide smoother and more robust information, beneficial for image post processing.

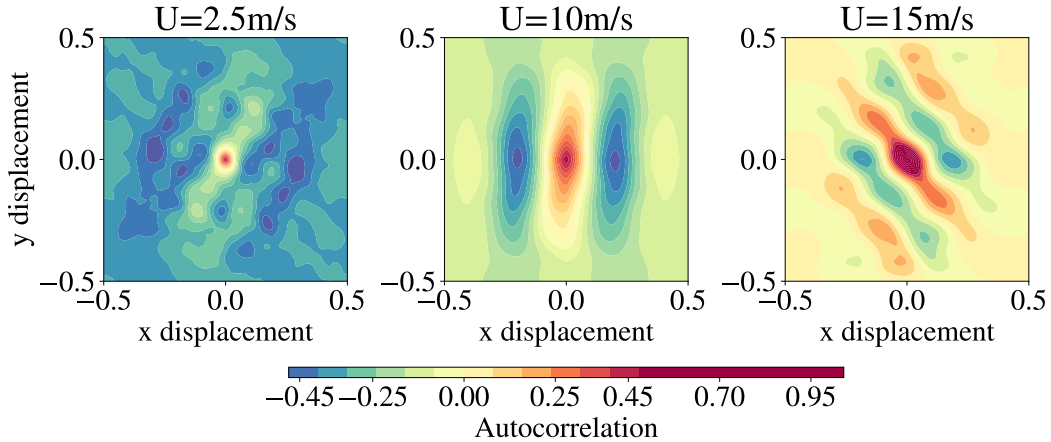


Figure 5. Normalized auto-correlation of PW image for the control case ($U=2.5\text{m/s}$), the optimal cal ($U=10\text{m/s}$), and the supercritical case ($U=15\text{m/s}$). These figures carry the orientation of the squall line, and have the advantage of being normalized and centered in 0. For each time step, an automatic post-process is therefore possible.

a direction X and as second axis Y, which has for length L and width W, the auto-correlation in $(x, y)(X, Y)$ will be equal to $(L - x/2)^2 * (W - y/2)^2$. The function is maximal at the center whatever the position of the band is, as a consequence of Cauchy-Schwarz theorem.

Figure 5 shows the autocorrelation of the precipitable water at convective radiative equilibrium, for the control ($U=2.5\text{m/s}$), optimal ($U=10\text{m/s}$) and supercritical ($U=15\text{m/s}$) cases. The function is normalized, and the colorbar is saturated to highlight the correlation area. We notice that the auto-correlation of PW is maximal in the center for the three cases. In the subcritical case, we have the characteristic signal of a white noise, random, since we observe a peak in the center and a fast diffusion of the signal. In the critical case, we observe the characteristic mark of a band, with a quadratic surface with two axes. The orientation is vertical, consistent with the PW figure. In the super-critical case, a similar pattern is observed, with the two axes oriented at an angle. By applying the autocorrelation filter, we obtain a reduced and centered representation of the convective organization. This first step will allow an automatic post-processing to measure the angle of the grain lines.

The questions we then asked ourselves were 1. how to measure the angle of the major axis of a pseudo quadratic shape, and 2. how to ensure that this angle is representative of a dynamic process, although in equilibrium. For the first question, we looked for an angle probability distribution for each image. The probability of an angle is defined as the distance between the autocorrelation pattern and a Gaussian filter. The Gaussian filter corresponds to the idealized image of a band, it is an approximation of a quadratic shape. We defined this Gaussian surface by a null mean $(0, 0)$ so that it is centered, and a covariance matrix $\sigma = [(1, -0.9), (-0.9, 1)]$, which defines a wide band of about twenty kilometers, and long of a hundred kilometers. This matrix corresponds to the width of an optimal line observed on the simulation sets. For each figure, we compute the dot product between its autocorrelation figure and our Gaussian filter for different angles. The range of angles is from -90 degrees to 90 degrees with respect to the vertical, with a precision of 3 degrees. Thus, for each autocorrelation image of PW, we have an angle distribution. Since we have a PW image for each time step (121 hours), we get an angle distribution.

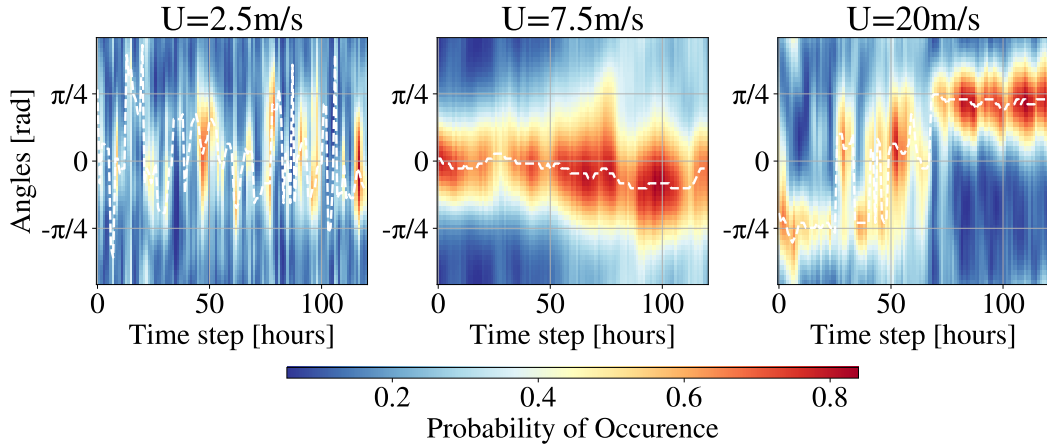
**Figure 6.** caption

Figure 6 shows the time evolution of the angle distribution for three cases, control ($U=2.5\text{m/s}$), near optimal ($U=7.5\text{m/s}$) and supercritical ($U=20\text{m/s}$). On the ordinate, we have the angle which varies from -90 degrees to 90 degrees with respect to the vertical, and on the abscissa, the time steps, from the RCE equilibrium to the end of the simulation (5 days). Each pixel represents the probability density of an angle at a given time. In white, the evolution in time of the most probable angle is plotted. In the control case, we notice that the distributions are very wide, and decorrelated from one instant of time to another. In the sub-critical case, we have peaks around 0 during the whole evolution. In the super-critical case, we have three periods, first peaks of probability at -50 , then a transition phase, and finally peaks in $+50$. This accounts for the indistinguishability between the 'top of the pool' and the 'bottom of the pool' for the projection of the angle, which sometimes gives rise to a broken line, similar to a so-called 'goose pate'.

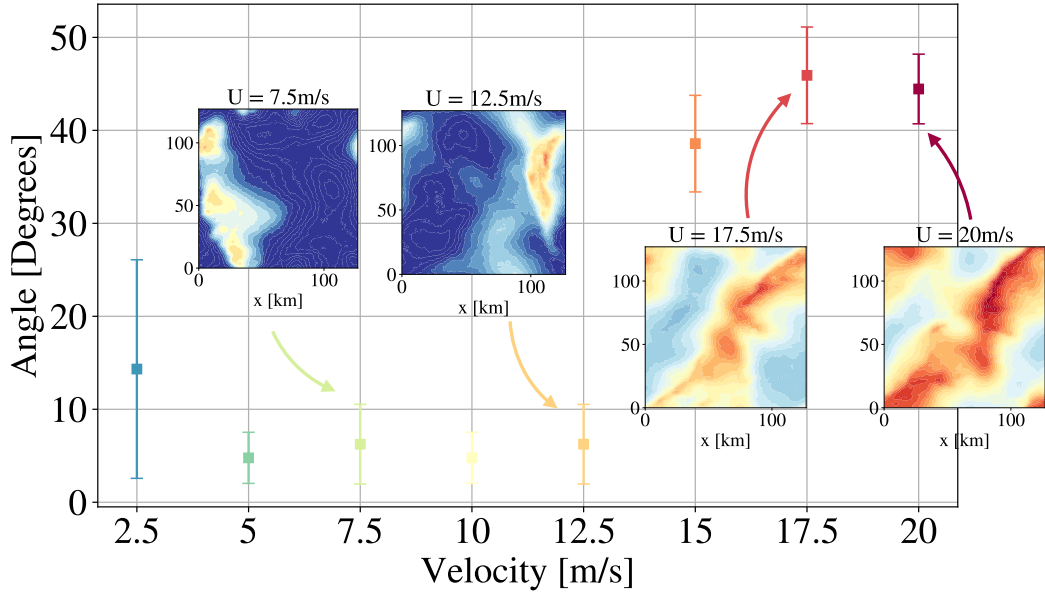
From the time evolution of the angle distributions for each simulation, we can determine an accurate angle. We first reduced the angle to values between $[0, \pi/2]$, taking its absolute value. Therefore, the final angle selected by our automatic method is the average over time of the absolute value of the most probable angle. We associate to each angle a measurement uncertainty, which corresponds to the variance of the distribution of the most probable angle (again in absolute value) in time.

Figure 7 provides a summary of the automatically measured angle for each case. The PW snapshots of the simulations are displayed to appreciate the angle measurement. This figure highlights 1. the absence of a precise angle for the control case; 2. two regimes of the squall lines, the sub-critical one, where the lines are perpendicular to the wind (an angle close to 0) and the super-critical regime where the lines are oriented from 40 degrees to 45 degrees; 3. a critical case for $U=12.5\text{m/s}$, the last case before the orientation of the line.

This method has been tested on several data sets and compared to repeated and rigorous manual measurements, which attests to the reliability of this approach. Now, we need to compare these measured angles to the theory of squall line orientation prediction.

3.3 Results and validation

The previous section has already validated several conclusions of the RKW theory on squall lines. First, the presence of a minimal shear threshold of line convection

**Figure 7.** caption

organization, which corresponds to the symmetry breaking described earlier. Second, we noted that there were two regimes, subcritical and supercritical, and that the lines were initially perpendicular to the wind and then oriented. We also observed that there was a critical shear at 12.5 m/s.

To test the theory of squall line orientation prediction, we plotted the projection of the basal shear velocity perpendicular to the squall line in Figure 8 for the different simulation cases. The basal velocity taken is the average over the entire domain of the longitudinal component of the surface velocity. The angle that the wind speed makes with the direction perpendicular to the line corresponds to the angle determined by our method (see diagram at the beginning).

On the figure, we have outlined what is predicted by the theory (in green). For the sub-critical regime, we should have an increasing line with a director coefficient equal to 1, which corresponds to a zero angle; the lines are perpendicular to the wind in order to maximize the cold pool and shear balance. This line reaches the critical case, for $U=12.5\text{ m/s}$, and at this moment, the wind speed and the pool speed are equal. We then enter the super-critical regime, and we expect saturation, i.e. the angle of the line maintains the cold pool/shear equilibrium. In orange, we have plotted the results of our simulations. We observe a very good agreement in the sub-critical regime with the lines almost merging. From the supercritical regime, we also have an interesting result which matches the theory with the error bars. At this stage, we can conclude that the theory of the conservation of the shear projection on the direction perpendicular to the grain line allows to predict the orientation angle of the convective bands.

However, there is some discrepancy between the theory and our results in the supercritical regime, and we wanted to understand if this was really due to measurement uncertainty or if some other phenomenon was at stake. In other words, we wanted to extend the theory to a higher order. For this, we were interested in the key element of the formation of grain lines, namely the cold pools, and this leads us to the next section.

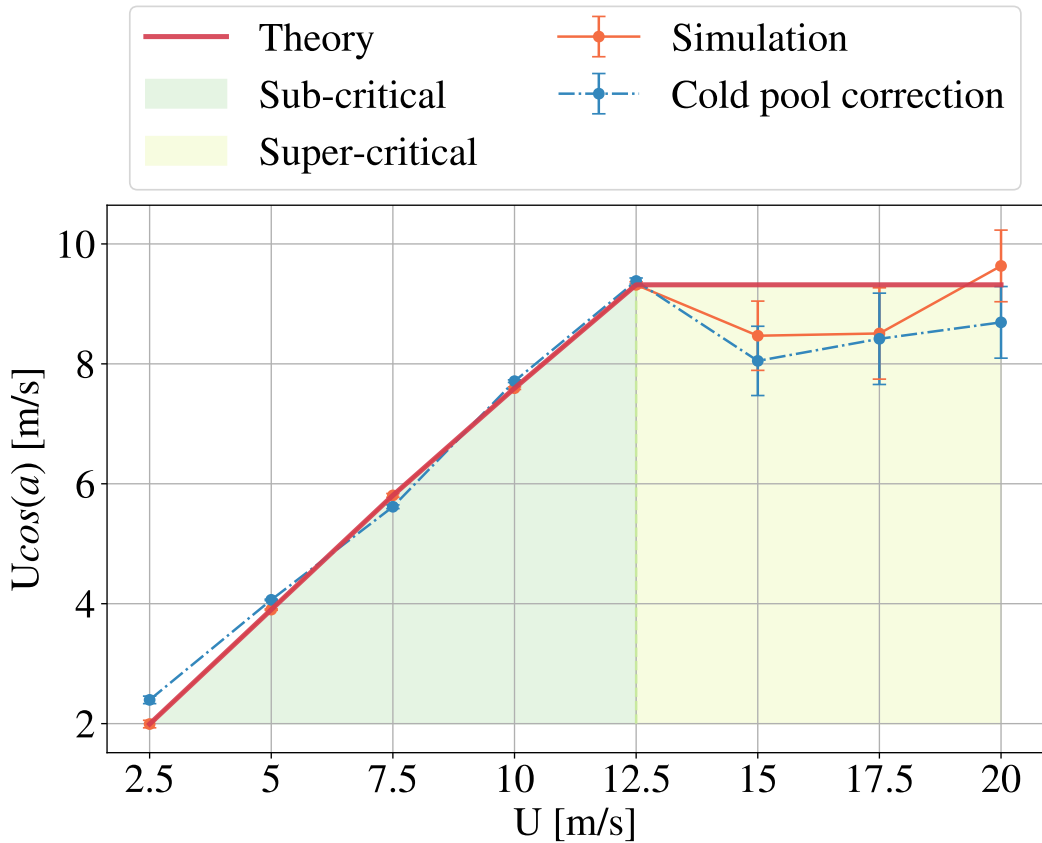


Figure 8. Evolution of the shear velocity projection perpendicular to the squall line, according to the 8 simulated cases. A very good agreement between the RKW theory and Robe Emmanuel, in green, our results, in orange is shown. We observe a saturation level, highlighting the subcritical and supercritical domain. The optimal state is found for $U=12.5\text{m/s}$. We took the effective imposed speed, which is lower than the theoretically imposed speed.

291 4 Investigation in cold pool properties evolution with shear

292 4.1 Statistical definition of cold pool

293 An interesting aspect of the squall lines and of the convective organization in general,
 294 is that the persistence of this particular form is linked to an intermittent phenomenon
 295 and perpetually repeated. In other words, it is the constant triggering of convective cells
 296 at the edges of the pools that manages to make a squall line subsist. Thus, to a convective
 297 band corresponds a multitude of cold pools. The squall lines are in some way the
 298 global result of a succession of local events.

299 The objective of this part is to study more in details the properties of the cold pools,
 300 and in particular to see how these properties evolved with the imposed shear. Among
 301 these properties we were interested in their height and temperature anomaly. Two meth-
 302 ods were then conceivable: either to gather a temporal and spatial collection of cold pools
 303 on which we will obtain a distribution on the properties; or to average directly on the
 304 pools, and to consider the properties of this 'mega-pocket' as representative of this mul-
 305 tiplicity. Conceptually, we define a global cold pools for each shear profile.

306 We have chosen the second method, and have calculated an average profile of cold
 307 pools for each imposed shear rate. Cold pockets are masses of cold air present especially
 308 after precipitation. The precipitating water evaporating cools the air and forms them.
 309 The existing literature represents temperature anomaly fields or buoyancy fields. The
 310 buoyancy is calculated as follows

$$311 B(x, y, z) = -g \frac{\theta'(x, y, z)}{\theta^*} \quad (2)$$

312 As we develop a statistical method for the analysis of the properties of the cold pools,
 313 we calculated the buoyancy in a composite way, i.e. we averaged in time this field, not
 314 according to a fixed position, but according to a fixed event whose position moves in time.
 315 It is although known that it is at the level of the maximum of precipitation that the pock-
 316 ets are the most active. Our anchor point of the calculation of average of composite is
 consequently the maximum of precipitation.

317 We were interested in the height of the pockets and the cold pocket shear equilib-
 318 rium front, so we took only xz sections to see the composite evolution of buoyancy as
 319 a function of altitude. Our composite image of buoyancy can be found in figure 9. These
 320 figures are centered at the maximum of precipitation in 0. In altitude, it rises until 1500m.
 321 The imposed wind arrives from the left to the right. On the top, it is the control case,
 322 and we observe a 'mega'-cold pocket symmetrical to the maximum precipitation and not
 323 very intense. In the case U=10m/s, we observe a dissymmetry of the pocket, which re-
 324 flects a resistance of the pocket to the frontal wind. Finally, at the bottom, for the su-
 325 per critical case U=15m/s, we observe the same dissymmetry, noting that the cold pools
 326 seems colder, and higher.

327 The conclusion of this figure is that when a shear wind is imposed, the pools are
 328 dissymmetric, and exhibit the same profile. It can also be noted that an intensification,
 329 in the sense of an increase in temperature anomaly and height, is taking place.

330 4.2 Intensification of cold pools

331 In this section, we will describe how to measure the cold pools intensification, and
 332 discuss its consequences on the cold pool-shear equilibrium that triggers the convective
 333 cells and the formation of squall lines.

334 We tried to quantify the energy of the cold pockets from our composite figures. The
 335 potential energy is defined as

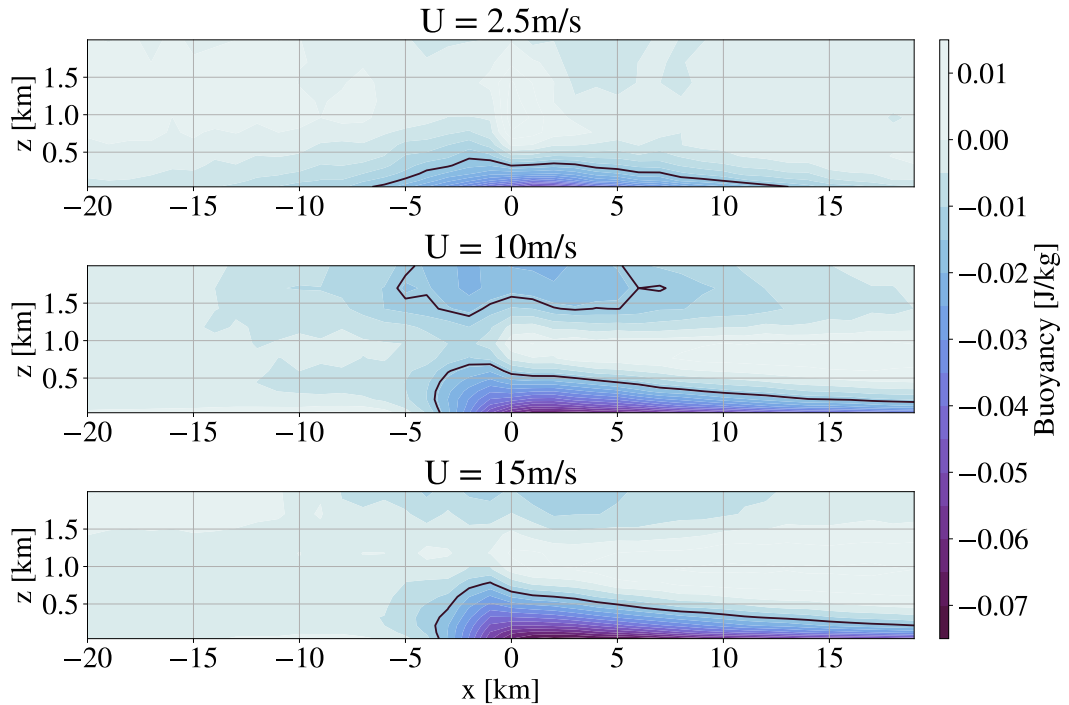


Figure 9. Composite image of the buoyancy in xz profile. The composite is performed at maximum precipitation, over 4 days of convective radiative equilibrium. In black, the boundary $b=-0.02\text{K}$ is drawn and delimits the cold pool. For the control case ($U=2.5\text{m/s}$), the cold pool is symmetric, with a maximum height of 500m. As the shear increases, we observe that the pool becomes higher and colder. This figure illustrates qualitatively the intensification of the cold pockets with the shear.

$$E_p = \int_{cp} B \quad (3)$$

336 where cp denotes the domain inside the cold pool. In our case, we tried to quan-
 337 tify the potential energy of the heart of the pockets, i.e. near the front. For that we cal-
 338 culated the potential energy as a function of the distance to the maximum precipitation,
 339 not to add an arbitrary constant in longitude. Figure 10 shows the potential energy of
 340 the cold pockets for each simulation case, as a function of the distance to the maximum
 341 precipitation. At the precipitation maximum, a gradual increase in potential energy is
 342 observed as a function of the imposed shear rate. This figure shows quantitatively the
 343 intensification of the cold pools, close to the precipitation maximum.

344 It is now a matter of understanding how this intensification is reflected in the cold
 345 pocket and shear balance. Does it allow to correct to a higher order the rotunno theory?
 346 In practical terms, how could the intensification of the pools impact significantly on the
 347 angle of squall lines?

348 The intensification of cold pools, insofar as they are associated with a higher prop-
 349 agation speed and could then move the position of triggering convective cells. More pre-
 350 cisely, if we make the hypothesis of a total transfer of potential energy to kinetic energy,
 351 we can deduce a propagation speed of the pools.

$$v_p = \sqrt{2E_p}. \quad (4)$$

352 Since the potential energy increases with the imposed shear (see figure 10), so does
 353 the velocity. We have taken into account this increase of velocity in the equilibrium in
 354 order to bring a correction to the current theory. For this purpose, we have plotted the
 355 following quantity

$$U\cos(a) - \Delta v_p \quad (5)$$

356 where Δv_p denotes the velocity deviation from the optimal case ($U=12.5\text{m/s}$). Fig-
 357 ure 8 shows in blue the correction brought by this calculation. For the subcritical regime,
 358 we still have the same agreement. For the supercritical case, we observe a correction. As
 359 we have seen an intensification of the pools, this results in a smaller angle than expected,
 360 and therefore the saturation level is lower. We conclude that the intensification of the
 361 pools is not a determining factor for the orientation of the squall lines.

362 4.3 Cause of cold pool intensification

363 This intensification, however, is real, and we wondered what the explanation was.
 364 We first questioned whether this intensification was due to the increase in height, or to
 365 the increase in the temperature anomaly. We therefore calculated the differential of the
 366 potential energy according to the height and the temperature. To do this, we developed
 367 the energy as follows

$$\Delta E_p = \Delta h(E_p/h) = \Delta E_p/h - E_p/h\Delta h + o(\Delta^2) \quad (6)$$

368 où Δ se calcule comme

$$\Delta\phi = \frac{\phi_{ctrl} - \phi}{\phi_{ctrl}} \quad (7)$$

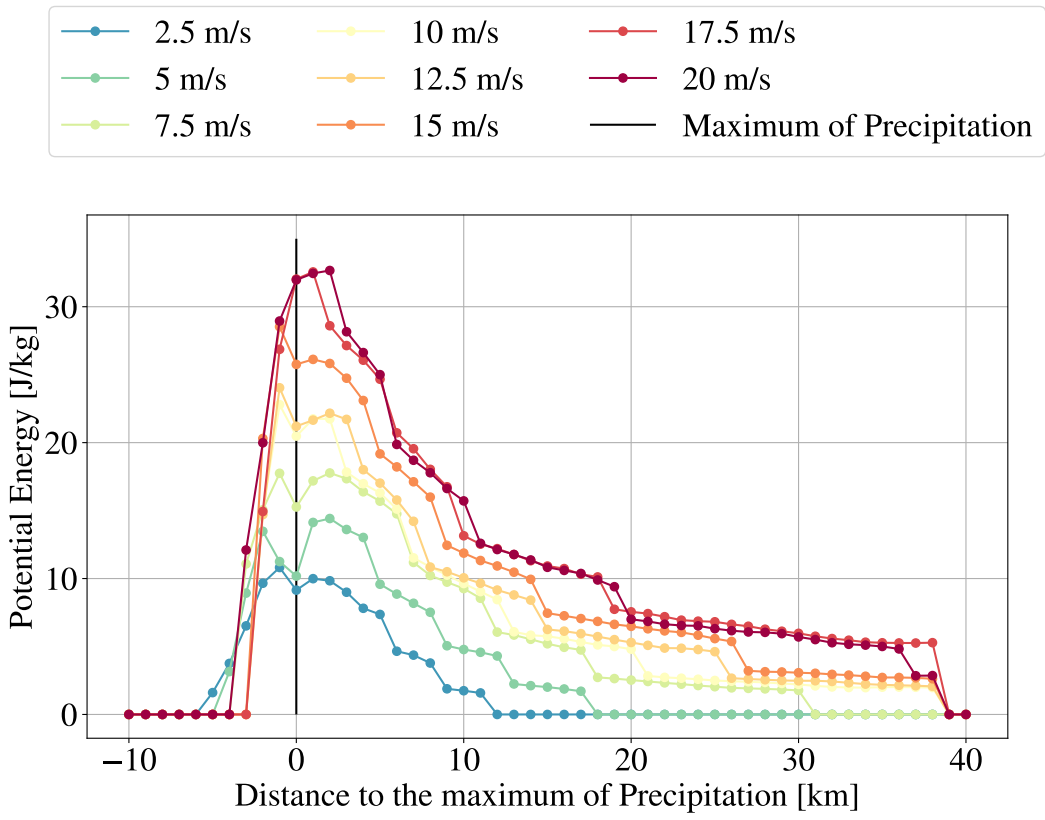


Figure 10. Potential energy of cold pools for each case as a function on the distance to the maximum of precipitation. The potential energy is computed for each x-step as the integral of the buoyancy up to the top of the composite cold pool. This figures shows a quantitative intensification of cold pools.

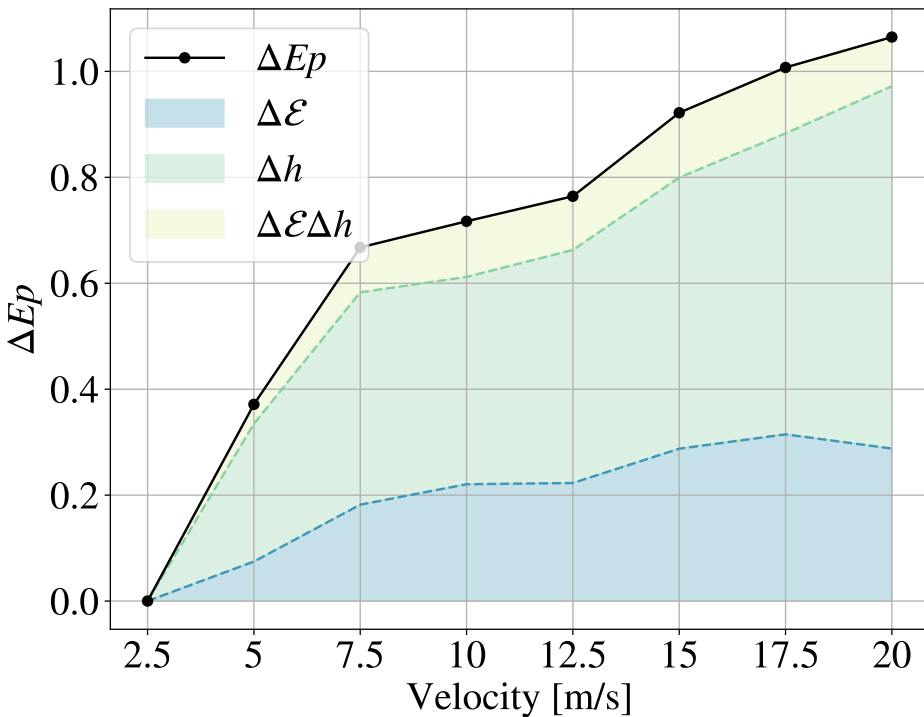


Figure 11. Evolution of the differential of the potential energy as a function of the cases. The differential is defined as $\Delta E_p = E_p - E_{p,ctrl}/E_{p,ctrl}$. For each simulation case, ΔE_p is decomposed as $\Delta E_p = \Delta E + \Delta h + \Delta E \Delta h$. This figure shows that the intensification of the cold pocket is the consequence of an extension in height.

et où Δ^2 désigne un terme du deuxième ordre. Dans notre cas, on ne peut pas négliger ce terme, qui est égal à $\Delta(E_p/h)\Delta(h)$.

Figure 11 shows for each case the decomposition of the differential of the potential energy. For example, for the case $U=20\text{ m/s}$, we see that the potential energy has doubled compared to the control case; it has increased by 20% compared to the optimal case. This figure shows that the evolution of the potential energy is mainly due to the increase of the height.

We investigated why the height of the pools increased with shear, and for this we were interested in rain evaporation. We hypothesized that rain evaporation occurred higher for high shear cases. So we took a closer look at the rain evaporation, QPEVP variable in the SAM model, which is a 3d variable, in g/kg. We constructed the composite figures for each case of this variable. In the same way as the previous composite figures, we averaged QPEVP centered on the precipitation maximum at each time step.

Figure 12 shows the isocontours QPEVP=-5g/kg, -10g/kg, -20g/kg and -50g/kg of the composite figures of rain evaporation. The more negative the value, the more intense the evaporation. At -5g/kg, this is the high, starting evaporation and -50g/kg is the lower, intense evaporation. We note that the rainfall evaporation for a given level is always higher for high shear cases. For example, if we take -5g/kg, we observe that the cases $U=15, 17.5$ and 20 m/s rise up to 7.5 km, while for the case control $U=2.5\text{ m/s}$,

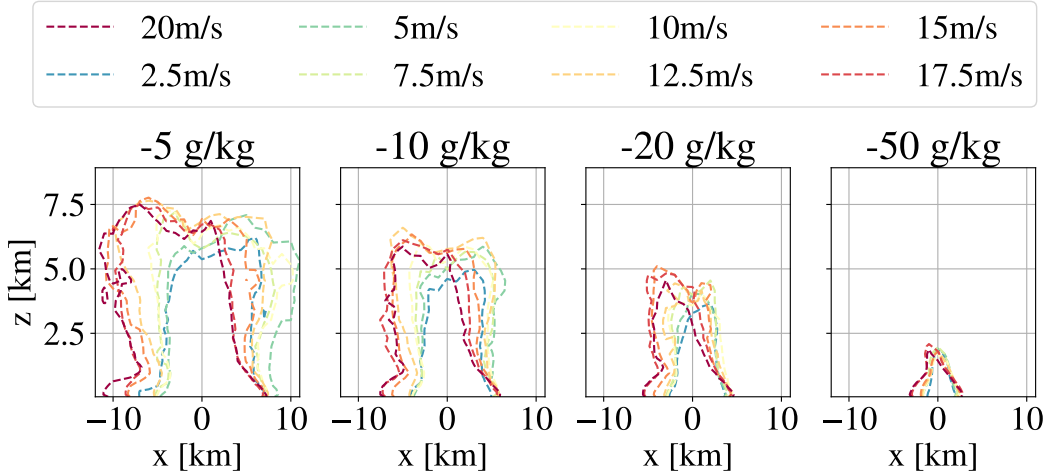


Figure 12. Isocontour of the composite evaporation of precipitation, of value -5g/kg , -10g/kg , -20g/kg , -50g/kg . These figures shows that the more shear, the higher the evaporation of rain starts. This can explain why cold pool are more intense as the shear increases.

388 the evaporation takes place at the highest at 6km. The difference decreases the closer
 389 one gets to the maximum precipitation on the ground. This study confirms that rain-
 390 fall evaporates higher with shear.

391 Now we just need to compare the height of the pools with the height of the rain-
 392 fall evaporation and see if there is indeed a correlation. We plotted the average profile
 393 of the QPEVP composites for each case in Figure 13. Specifically, we computed the rain-
 394 fall evaporation composites in xz section, and then averaged along the x direction (over
 395 20km) to obtain the desired profile. Also, we show here only the profiles up to 1400m,
 396 that's why the values are from -20 to -65 g/kg . On this figure, we have also plotted the
 397 evolution of the height of the cold pools for each case. We took the average of the height
 398 on 5km at the front of pools. We notice that the evolution of the height of the pools fol-
 399 lows with a good agreement the isocontour of the rain evaporation. The hypothesis ac-
 400 cording to which the height of the evaporation of rains is at the origin of the increase
 401 in height of pockets is thus validated.

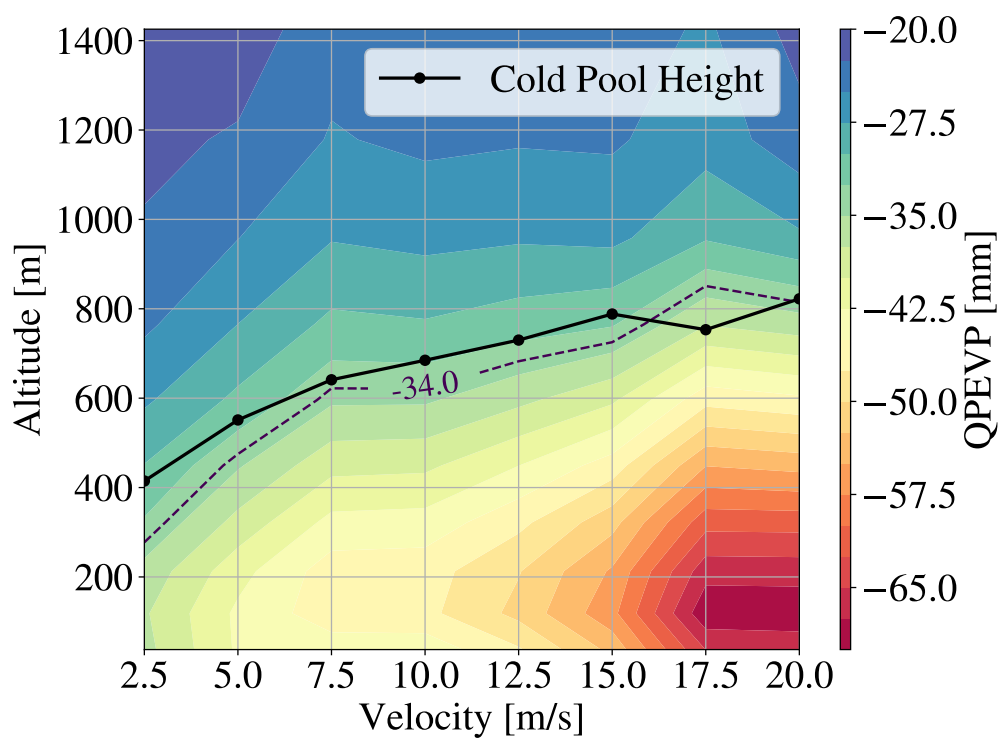


Figure 13. caption

402

U	Basal velocity in wind shear profile, from 2.5 to 20 m/s
H	Depth shear of wind shear profile equal to 1000 m
x	longitudinal direction
y	latitude
z	altitude
t	time
W	Vertical velocity [m/s]
PW	Precipitable water [mm]
QN	Cloud humidity
QP	Precipitative water
QPEVP	Rain evaporation
TABS or θ	Absolute Temperature
θ'	Temperature Anomaly
α	Angle of the squall line regarded to the vertical
g	gravity [m/s ²]
B	Buoyancy [J/kg]
E_p	Potential energy of cold pools
v_p	Propagation velocity of cold pools
Δv_p	Gap between optimal propagation velocity

403

5 Discussion

404

Acknowledgments

405

Enter acknowledgments, including your data availability statement, here.